The speciation and mobility of Mn and Fe in estuarine sediments

Authors: Véronique E. Oldham[1*], Matthew G. Siebecker[1ɣ], Matthew R. Jones[2≠], Alfonso Mucci[3], Bradley M. Tebo[2], George W. Luther III[1]

Affiliations:

[1]School of Marine Science and Policy, University of Delaware, Lewes, DE, 19958

[2]Division of Environmental and Biomolecular Systems, Institute of Environmental Health, Oregon Health & Science University, Portland, OR 97239

[3]GEOTOP and Department of Earth and Planetary Sciences, McGill University, Montreal, QC, H3A 0E8

Current addresses

*Department of Marine Chemistry and Geochemistry, Woods Hole Oceanographic Institute, Woods Hole, MA, 02543

[≠]POSTECH – Pohang University of Science and Technology, Division of Environmental Science and Engineering, Pohang-si, Gyoungsangbuk-do, 37673, Korea

[ɣ]Department of Plant and Soil Science, Texas Tech University, Lubbock, TX, 79409, USA

*Correspondence to: voldham@whoi.edu

"This is a post-peer-review, pre-copyedit version of an article published in Aquat Geochem . The final authenticated version is available online at: https://doi.org/10.1007/s10498-019-09351-0".

Abstract

Dissolved and solid phase speciation of Mn and Fe were measured in the porewaters of sediments recovered from three sites in the Greater St. Lawrence Estuary: the Saguenay Fjord (SAG), the Lower St. Lawrence Estuary (LSLE) and the Gulf of St. Lawrence (GSL). At all sites and most depths, metal organic ligand complexes (Mn(III)-L and Fe(III)-L) dominated the sedimentary porewater speciation, making up to 100 % of the total dissolved Mn or Fe. We propose that these complexes play a previously underestimated role in maintaining oxidized soluble metal species in sedimentary systems and in stabilizing organic matter in the form of soluble metal-organic complexes. In the fjord porewaters, strong ($\log K_{COND} > 13.2$) **and weak (**$\log K_{COND} < 13.2$) **Mn(III)-L complexes were detected, whereas only weak Mn(III)-L complexes were detected at the pelagic and hemi-pelagic sites of the GSL and LSLE, respectively. At the fjord site, Mn(III)-L complexes were kinetically stabilized against reduction by Fe(II), even when Fe(II) concentrations were as high as 57 µM. Only dissolved Mn(II) was released from the sediments to overlying waters, suggesting that Mn(III) may be preferentially oxidized by sedimentary microbes at or near the sediment-water interface. We calculated the dissolved Mn(II) fluxes from the sediments to the overlying waters to be 0.24 µmol cm^{-2} yr^{-1} at the pelagic site (GSL), 11 µmol cm^{-2} yr^{-1} at the hemi-pelagic site (LSLE), and 2.0 µmol cm^{-2} yr^{-1} in the fjord. The higher benthic flux in the LSLE reflects the lower oxygen concentrations (dO_2) of the bottom waters and sediments at this site, which favor the reductive dissolution of Mn oxides as well as the decrease in the oxidation rate of dissolved Mn(II) diffusing through the oxic layer of the sediment and its release to the overlying water.**

1 Introduction

The redox chemistry of marine sediments plays a major role in global elemental cycling and serves as an indicator of global climate change (e.g. Hedges and Keil, 1995). Redox-sensitive elements, such as manganese (Mn) and iron (Fe), have been used as tracers of processes that affect the concentration of atmospheric CO_2 and the global carbon cycle since they participate in the remineralization of sedimentary organic carbon (e.g. Canfield et al., 1993). The transformation of sedimentary organic carbon to CO_2 proceeds through a combination of diverse respiratory and fermentative pathways that are ultimately balanced by the reduction of inorganic electron acceptors: O_2, NO_3^-, Mn and Fe oxides and SO_4^{2-}. Thus, to better understand and model organic carbon oxidation, a characterization of the speciation (redox state and complexation) and reactivity of each electron acceptor along sedimentary redox gradients is critical.

After the depletion of dissolved oxygen (dO_2) in sediments, NO_3^-, Mn oxides and Fe oxides become, sequentially, the thermodynamically preferred electron acceptors in the microbial decomposition (i.e., mineralization) of organic carbon (Froelich et al., 1979; Gaillard et al., 1989; Van Capellen and Wang, 1996; Luther et al., 1997). The mineralization of organic carbon by Mn and Fe is thought to proceed via reduction and solubilization of solid Mn(III/IV) and Fe(III) oxides, but the presence of more readily bioavailable and soluble Mn(III) and Fe(III) species could accelerate the mineralization of organic carbon (Lin et al., 2012). Soluble Fe(III)-L complexes have been measured in salt marsh sediments (Luther et al., 1992, 1996) and in anoxic sediments (Beckler et al, 2015, Taillefert et al., 2000, 2002) and are considered the dominant soluble species of Fe in open ocean waters (e.g. van den Berg, 1995). In marine systems, Mn speciation is comprised of dissolved Mn(II), Mn(III) and solid Mn(III/IV) oxides (MnO_x). Until the last decade, it was thought that soluble Mn was predominantly found as free-hydrated Mn(II), but the presence of Mn(III)-L (where L denotes a complexing ligand) complexes has since been found to be a major, if not the major, component of soluble Mn species in low oxygen environments (Trouwborst et al, 2006; Yakushev et al., 2007, 2009; Madison et al., 2011; Dellwig et al., 2012; Oldham et al., 2015) including suboxic sediment porewaters (Madison et al., 2013) and, more recently, in oxic systems (Oldham et al., 2017a, 2017b, 2017c). Because Mn(III)-L complexes can donate or accept electrons, accounting for their presence in marine

sediments is critical when assessing organic carbon budgets and the redox capacity of a sedimentary system (Yakushev et al., 2007, 2009; Madison et al., 2013). Additionally, Mn(III) can bind to the same ligands as Fe(III) (Duckworth and Sposito, 2005, 2007; Parker et al., 2004, 2007; Luther et al., 2015) and, thus, its presence could disrupt the mobility and biotic uptake of Fe in regions where the latter are facilitated by the solubilization and binding of Fe to organic ligands. Given that the reactivity and speciation of Mn and Fe are also pH and Eh dependent (Stumm and Morgan, 1996; Luther, 2010), marine sediments host a dynamic Mn and Fe chemistry with the extent of diagenetic remobilization ultimately driven by the oxidant demand of the sediment.

In this study, we primarily examined the speciation of Mn in the sediment porewaters at three sites (Fig. 1). Each site had different overlying water dissolved oxygen (dO_2) concentrations and organic carbon accumulation rates: from land to sea, the first site was in the Saguenay Fjord (SAG-30), a tributary of the Lower St. Lawrence Estuary (LSLE); the second in the LSLE (Station 23); and third in the Gulf of St. Lawrence (GSL, Station 17). The greater St. Lawrence Estuary is the largest estuary in the world, and the outlet of the Great Lakes to the Atlantic Ocean. The dominant bathymetric feature of the LSLE and GSL is the Laurentian Trough (or Channel), a 300+ m deep U-shaped valley that extends 1250 km from the continental shelf break to the head of the LSLE at Tadoussac. In the summer months, the water column of the LSLE and the Gulf is characterized by a three-layered structure separated by two sharp temperature inversions (Dickie and Trites, 1983; El-Sabh and Silverberg, 1990). Bottom-water dO_2 concentrations decrease as North Atlantic water flows landward along the Laurentian Trough from Cabot Strait (Gilbert et al., 2005).Consequently, bottom-waters at Station 23 are severely hypoxic (dO_2< 60 μM), whereas bottom-water dO_2 concentrations at Station 17 in the GSL are ~130 – 200 μM. Factors responsible for the recent development of hypoxic bottom waters in the LSLE are discussed in Gilbert et al. (2005), Thibodeau et al. (2006) and Genovesi et al. (2011). Organic carbon accumulation rates along the Laurentian Trough increase landward nearly 50-fold (see Benoit et al. (2006) for a compilation). The combined decrease in bottom-water oxygenation and increased organic carbon accumulation rates may lend itself to greater release of Mn from the sediments and increase its long-range transport because abiotic Mn(II) oxidation

rates and precipitation of Mn(III/IV) oxides will decrease as dO_2 concentrations decrease (Stumm and Morgan, 1970).

The Saguenay Fjord study site (SAG-30, Fig. 1) is within a 103 km long fjord, which is ~3 km wide, up to 270 m deep, and connects with the LSLE through a 22-m deep sill. Detailed descriptions of the physiographic features of the Saguenay Fjord can be found in Schafer et al. (1990) and Locat and Levesque (2009). The water column of the fjord is characterized by a sharp pycnocline that separates two distinct water masses. The thick bottom layer is well-mixed and well-oxygenated (~300 μM dO_2), with waters penetrating landward from the St. Lawrence Estuary as they episodically spill over the sill (Stacey and Gratton, 2001; Bélanger, 2003; Belzile et al., 2014). Bottom-water practical salinities (S_P) are approximately 30.5 (Mucci et al., 2000), with temperatures ranging from 0.4 to 1.7 ºC (Fortin and Pelletier, 1995). The 8 - 10 m thick surface layer consists of brackish waters (S_P~0 – 10) resulting from the turbulent mixing of the outflow from the Saguenay River and the underlying marine waters. Detailed hydrographic characteristics of the fjord can be found in Schafer et al. (1990) and Gratton et al. (1994).

Previous studies have indicated that Mn is a dominant redox-active element in the upper sediment at Station 23, with MnO_x concentrations exceeding 100 μmol g^{-1} (Anschutz et al., 2000; Madison et al., 2013). In addition, Madison et al. (2013) observed that porewater soluble Mn(III) is a major component of the sedimentary redox system of the St. Lawrence Estuary, including Station 23, and the Gulf of St. Lawrence. In this paper, we report vertical sediment profiles of Mn speciation at Station 23 as well as profiles at Station 17, a more pelagic site, and at SAG-30, a more terrestrially influenced site, in the Saguenay Fjord. Furthermore, we added a protocol to distinguish weak from strong Mn(III) binding ligands (Oldham et al., 2015). Based on previous findings in coastal waters, terrestrially-derived ligands form strong Mn(III)-L complexes (log K_{COND} > 13.2; Luther et al., 2015; Oldham et al., 2017a, 2017b, 2017c) and these were found to comprise up to 70 % of the total dissolved Mn in the water column at SAG-30,

while [Mn(III)-L] reached a maximum of 484 nM ~10 m above the sediment-water interface (Oldham et al., 2017a).

In addition to dissolved Mn and Fe speciation measurements, we determined the concentrations of solid-phase Mn and Fe following an ascorbate leach as well as the concentration of porewater dO_2 via voltammetric electrode profiling. Results from this study were used to refine our understanding of the geochemical behavior of Mn during early diagenesis, including factors that control its remobilization to the overlying waters.

2. Materials and Methods

2.1 Porewater sampling and processing

Undisturbed sediment cores were recovered using a 0.12 m^2 Ocean Instruments Mark II box corer, in September 2014, from the Lower St. Lawrence Estuary (Station 23), the Gulf of St. Lawrence (Station 17) and the Saguenay Fjord (SAG-30) (Fig. 1). The entire area of the cores was immediately sectioned, in a nitrogen-purged glove box (Edenborn et al., 1986) to avoid oxygen contamination, at depth intervals of 0 – 0.5 cm, 0.5 – 1 cm, 1 – 2 cm, 2 – 3 cm, 3 – 4 cm, 4 – 5 cm, 5 – 7 cm, 7 – 9 cm, 9 – 11 cm, 11 – 13 cm, 13 – 15 cm, 15 – 18 cm, and 18 – 21 cm. Fractions of these sections were transferred to modified Reeburgh squeezers (Reeburgh, 1967) and extracted porewaters filtered in-line through a 1 μm nominal pore size microfiber glass filter and a 0.45 μm HA mixed cellulose Millipore membrane filter as they passed directly into 50 mL pre-cleaned plastic syringes with Teflon-covered plungers. The porewater syringes were transferred to an argon-filled glove bag and samples filtered again through 0.2 μm Nylon Millipore syringe filters into new 50 mL centrifuge (Falcon) tubes.

Overlying water samples were recovered with undisturbed sediments using a Bowers & Connelly multi-corer, were syphoned off the top of the core using a syringe and clean PFTE tubing and transferred directly into clean 50 mL centrifuge tubes. We note that these overlying waters are not altered on the way up through the water column as the corer is sealed. These samples were immediately filtered through 0.2 μm Nylon Millipore syringe filters into new 50 mL falcon tubes. Samples were kept in an argon atmosphere until analysis and were analyzed within 4

hours of collection for Mn speciation and total dissolved Mn (dMn_T), as indicated in the next section. In addition, microelectrode profiling (section 2.7) was performed on one of these multi-cores from each site.

The total carbon (TC) and total nitrogen (TN) contents of the sediment were determined using a Carlo Erba™ NC 2500 elemental analyzer, as described in Thibodeau et al. (2006). The reproducibility of the analyses was estimated at ± 0.1 % for TC and ± 0.3 % for TN, based on replicate measurements of standard substances. The inorganic carbon (IC) content of the freeze-dried sediment was measured by coulometric titration using a UIC coulometer following acidification of the samples and CO_2 extraction. The analytical reproducibility was better than 2 %. The organic carbon (OC) content of the sediment was calculated from the difference between the TC and IC concentrations.

The mass accumulation and organic carbon accumulation rates were calculated from the sedimentation rates (Smith and Schafer, 1999; Barbeau et al., 1991; Smith and Walton, 1980) and the sediment porosity. The latter was determined from the water content of the sediments, the salinity of the corresponding bottom water and a dry sediment density of 2.65 g/cc. The water content was determined from the change in weight after freeze-drying of an aliquot of the wet sediment (Lefort et al., 2012).

2.2 Dissolved Mn speciation

All 0.2 μm filtered samples were analyzed for soluble Mn speciation (eq. 1) within 4 hours of porewater processing following the addition of a soluble porphyrin ligand as a colorimetric agent, a method described by Madison et al. (2011).

$$dMn_T = Mn(II) + Mn(III)L_{weak} + Mn(III)L_{strong} \quad (1)$$

The method allows for the subsequent determination of both Mn(II) and Mn(III)-L_{weak} using the differential kinetics of the reaction between Mn and the added Cd-substituted porphyrin. The Mn(II) reacts rapidly with the porphyrin, forming a Mn(III)-porphyrin complex in the presence

of oxygen, whereas the Mn(III)-L_{weak} undergoes a slower ligand substitution reaction with the porphyrin to form the Mn(III)-porphyrin complex (log K_{cond} <13.2, Luther et al., 2015). The Mn(III)-porphyrin complex yields a sharp Soret band at 468 nm (ε = 94,600 mol^{-1} cm^{-1}), which is measured over the course of the reaction (15 minutes) using a Hewlett Packard 8452B diode-array spectrophotometer (2 nm wavelength resolution) controlled by Olis, Inc. Globalworks software. The peak that develops over the course of reaction with a natural sample is fitted to a 4-parameter double exponential equation which can be solved to determine the Mn(II) and Mn(III)-L_{weak} concentrations. From the kinetics of these analyses, conditional stability constants of the Mn(III)-L_{weak}, can be determined. A formation constant (k_1) for the reaction of Mn(II) with the porphyrin is solved using a reduced sample containing only Mn(II) [converting all dMn_T to Mn(II)] and a single parameter rise to a maximum (Madison et al., 2011). Based on this kinetic curve and our kinetic curve of unreduced sample containing Mn(II) and Mn(III)-L_{weak}, we solve for k_2, which is the dissociation constant of the Mn(III)-L_{weak} (k_d). We then use the water exchange rate of Mn(III) as a conservative estimate of the Mn(III)-L_{weak} formation constant (k_f); this allows us to solve for K_{cond}, which is equal to k_f/k_d. A detailed description of the solution to the reaction kinetics is found in Madison et al. (2011) and Luther et al. (2015). To measure Mn(III)-L_{strong} (log K_{cond} >13.2), a reducing agent (hydroxylamine, 100 times excess of expected dMn_T) is added to the filtered sample, converting all Mn(III)-L to Mn(II), and the sample is reanalyzed for dMn_T (Oldham et al., 2015). The Mn(III)-L_{strong} concentration is obtained from the difference between the reduced and non-reduced sample analyses. Colloidal MnO_2 does not react with the porphyrin, as shown by Madison et al. (2011). The detection limit for this method is 50 nM, which is sufficiently low for porewater analysis.

2.3 Ascorbate Mn and Fe extractions

Mn(asc) and Fe(asc) were determined after extraction of the ground, freeze-dried sediment in a pH 8 buffered ascorbic acid solution (Ferdelman, 1988; Kostka and Luther, 1994) at a solid:solution ratio of 1:50 for 24 hours on a wrist shaker. This reagent reduces and dissolves the amorphous Fe oxide phases that are available to dissimilatory Fe-reducing bacteria (Kostka and Luther, 1994; Hyacinthe et al., 2006) and quantitatively extracts sedimentary Mn oxide phases (Anschutz et al., 2005; Lefort et al., 2012). Note that results of this Mn extraction are identical to

those obtained after extraction in a 1 M hydroxylamine–hydrochloride and 25 % (v/v) acetic acid solution (Chester and Hughes, 1967) or 1 N HCl solution (Leventhal and Taylor, 1990; Raiswell et al., 1994).

The concentrations of Fe and Mn in the ascorbate extracts were determined by flame atomic absorption spectroscopy on a Perkin-Elmer, model AA100 Atomic Absorption Spectrometer. The instrument was calibrated with external standards prepared by dilution of a certified 1,000 ppm stock solution (Fisher Scientific AAS certified standard). The reproducibility of the measurements was better than 5 % for both Mn and Fe, and the detection limits were, respectively, < 0.01 μmol/g and < 0.02 μmol/g. The reproducibility of the buffered ascorbic acid extraction procedure is typically ± 3 % for Mn and ± 7 % for Fe (Chaillou et al., 2003).

2.4 Flux calculations

To estimate the flux of dMn_T from the sediment to the overlying waters, we applied Fick's Law using a vertical diffusion coefficient of 3.75×10^{-10} m^2 s^{-1} (Schulz, 2000), an average porosity of 0.9 for these sediments (as used in Mucci et al. 2003), and a linear concentration gradient between the average concentrations in the top 0.5 cm of the sediments and the overlying waters.

The Mn(asc) and Fe(asc) accumulation rates are calculated from the integrated amount of Mn(asc) and Fe(asc) in the sediment (μmol per gram of sediment) over the length of the core multiplied by the mass accumulation rate (MAR; gram of sediment cm^{-2} yr^{-1}). In turn, the mass accumulation rate is calculated for each sampling interval from the sedimentation rate (cm yr^{-1}) and the mass of solids per unit volume of sediment (= (1-ø)*2.71 where ø is the porosity; g cm^3). The Mn(asc) and Fe(asc) burial rates are obtained from the average concentration of Mn(asc) and Fe(asc) in the sediment over the length of the core below the active zone (i.e., top 10 – 15 cm) multiplied by MAR (or the average Mn(asc) and Fe(asc) content of the sediment deposited in one year in the bottom layers of the core).

2.5 Total dissolved Mn and Fe concentration determinations by Flame-AAS

Total dissolved Mn and Fe concentrations were determined for each sampled sediment-depth interval on filtered (0.45 μm) porewaters. Aliquots were acidified with a 1 % equivalent volume of ultrapure, concentrated HNO_3 (Seastar) (pH<1.5) and kept refrigerated until analysis. Porewater analysis was conducted as described above for the ascorbate extracts (Section 2.4). Detection limits for dMn_T and dFe_T were, respectively 1 and 2 μM and the reproducibility was better than 5 %.

2.6 Dissolved Fe(II)

Porewater samples were analyzed for dissolved Fe(II) using the Ferrozine method of Stookey (1970). Samples were stored in an argon-filled glove bag until analysis on the same day. In this method, Fe(II) reacts to form a purple complex whose absorbance was measured at 562 nm, in a 1-cm quartz cell, using the diode-array spectrophotometer described in section 2.2. The detection limit for this method is 100 nM using a 1-cm cell, with an average reproducibility better than 4 %. The concentration of Fe(III)-L complexes was obtained from the difference between the total dissolved Fe determined by AAS and Fe(II) by ferrozine.

2.7 Voltammetric profiling of dO_2

A solid-state gold-amalgam glass microelectrode (Brendel and Luther., 1995: Luther et al., 2008) coupled to a potentiostat (DLK60, Analytical Instrument Systems, Inc.) was used to measure dissolved oxygen profiles in sediment cores from the multi cores (Luther et al., 2008). The position of the electrode was controlled using a micromanipulator with a 0.1 mm resolution capability. Scans were performed using cyclic voltammetry across a potential of -0.05 to -1.8 V at a 1000 mV s^{-1} scan rate with a conditioning step of -0.05 V applied for 2 seconds at the beginning of each scan. No H_2S was present at the depths analyzed in this study. The detection limit for this method is 0.2 μM H_2S and 3 μM dO_2.

3 Results

Results of the speciation analyses from this study at all 3 sites can be found in Figure 2 and Table 1. The results focus on dMn_T measured using the porphyrin method rather than AAS, for reasons discussed in section 3.5.

3.1 Station 17

The top three panels of Figure 2 show our results from Station 17, and the results for Mn and Fe speciation are summarized in Table 1. The water directly overlying the sediment-water interface at Station 17 contained 127 ± 2 μM dO_2, which rapidly decreased to 55 ± 3 μM within the top 0.5 cm of the sediments, before falling below our detection limit beyond 1.0 cm depth. Below the oxygen penetration depth, we observe the solid-phase Mn(asc) maximum of 63 μmol g^{-1}, which decreases to ~1 μmol g^{-1} below 3 cm depth. The maximum solid-phase Fe(asc) concentration (71 μmol g^{-1}) appears within the 1.0 – 2.0 cm depth interval, slightly below the Mn(asc) maximum. The Fe(asc) is 51 – 71 μmol g^{-1} in the top 2 cm of the sediments, compared to 7.8 – 63 μmol g^{-1} for Mn(asc), and below 2.0 cm, Fe(asc) decreases steadily from 16 to ~ 10 μmol g^{-1}.

Despite higher solid phase Fe concentrations, the porewater dFe_T concentration is lower than that of dMn_T at all depths. Coinciding with the disappearance of Mn(asc) (and MnO_x) at depth is the appearance of soluble Mn, which increases from 1.9 – 2.7 μM in the top 3 cm of sediment to 29 – 48 μM below 3 cm, whereas dFe_T ranges from non-detectable to 13 μM in the same interval. Mn(III)-L_{weak} accounts for 100 % of the dMn_T between 2.0 – 9.0 cm, and 84 – 89 % between 15.0 – 21.0 cm. Within the 9.0 – 15.0 cm sediment depth interval, Mn(II) comprises 100 % of the dMn_T, which coincides with a ~2 – 4 μM increase in the dFe_T. The dFe_T speciation is also dominated by organic complexation, with Fe(III)-L complexes comprising the entire soluble fraction in all samples.

3.2 Station 23

At Station 23, the dO_2 was 57 ± 2 μM in waters above the sediment-water interface and it decreased to non-detectable levels below 0.5 cm. The solid phase Fe(asc) concentration (71 – 152 μmol g^{-1}) is significantly higher at all depths than Mn(asc) (3.4 – 38 μmol g^{-1}). The

subsurface Mn(asc) maximum occurs directly at the sediment-water interface (i.e., 0 – 0.5 cm depth interval), whereas the Fe(asc) maximum is found at 3.0 cm. The Mn(asc) concentration decreases rapidly to < 5 μmol g^{-1} below 2.0 cm (10 times lower than the maximum concentration), whereas the Fe(asc) decreases more steadily, from 87 to 71 μmol g^{-1}, below 3.0 cm (half as much as the maximum concentration).

The concentration of dMn_T exceeded dFe_T at all depths. The dMn_T was 110 μM at the sediment-water interface and increased to 213 – 237 μM in the depth range of 0.5 to 3.0 cm. In contrast, dFe_T was not detectable until 1.0 cm, and increased from 16 μM within the 2.0 – 3.0 cm interval to a maximum of 105 μM at 7.0 – 9.0 cm. No strong Mn(III)-L complexes were detected at this site, but Mn(III)-L_{weak} was present at most depths. Where the dMn_T was higher than 150 μM, % Mn(III)-L_{weak} was greater than 48 % (48.7 – 87.0 %) whereas, when dMn_T was below 150 μM, the % Mn(III)-L_{weak} was lower (22.6 – 37.8 %). With the exception of the surface sediments, the lower % Mn(III)-L corresponded to the subsurface dFe_T maximum (70 – 105 μM, 4.0 – 9.0 cm). We measured Fe(III)-L complexes at all depths where dissolved Fe was detected (except within the 11.0 – 13.0 cm interval) and it comprised 35 – 75 % of dFe_T.

3.3 The Saguenay Fjord

The water overlying the sediments at the Saguenay Fjord station (SAG-30) contained 231 ± 4 μM dO_2 which decreased to 66 ± 2 μM within the 0 – 0.5 cm interval before reaching non-detectable levels below 1.0 cm depth. At this site, we observed the highest Fe(asc) concentrations (200 – 362 μmol g^{-1}) and lowest Mn(asc) concentrations (2.3 – 33 μmol g^{-1}) of all three sites. Here, the subsurface Fe(asc) and Mn(asc) maxima coincided and were found within the first sediment sampling interval (0 – 0.5 cm). Fe(asc) decreased steadily to about 2/3 of the surface concentration by 21.0 cm depth, whereas Mn(asc) decreased by a factor of 10 from the surface to 21.0 cm.

dFe_T and dMn_T increased downcore from the top 0.5 cm of sediment (Fig. 2). Below 0.5 cm, dFe_T increased sharply from 26 – 77 μM within the 1.0 – 3.0 cm depth intervals, peaking at nearly 300 μM within the 5.0 – 7.0 depth interval and varying between 155 and 296 μM below.

The porewater dFe_T is dominated by Fe(III)-L complexes, which make up 60.4 – 87.6 % of the total, throughout the sediment profile. Likewise, the dMn_T concentration increases above 100 µM within the 3.0 – 5.0 interval, and remains relatively constant below, but the soluble Mn speciation is more variable. Mn(III)-L complexes comprise 60 – 100 % of the dMn_T and both strong and weak Mn(III)-L complexes were detected, with strong complexes comprising up to 16 % of the dMn_T. Below 13.0 cm depth, the dMn_T decreased slightly from 51 – 83 µM while weak Mn(III)-L complexes were non-detectable. In other words, only Mn(II) and strong Mn(III)-L complexes (7 – 16 % of dMn_T) were present below this depth.

3.4 Dissolved Mn and Fe fluxes

Table 2 summarizes the fluxes of Mn and Fe to and from the sediments at our three study sites, along with values obtained during previous studies (Silverberg et al., 1987; Lefort et al., 2012; Mucci, unpublished) at these sites and six nearby sites in the St. Lawrence Estuary. Sites 24, 20, 18, 16, Cabot Strait (CS) and entrance to the Laurentian Channel (ECL), are progressively seaward in that order and reach the mouth of the Laurentian Channel at the continental shelf break (Fig. 1).

We calculated an upward diffusive flux of Mn(II) from our three study sites. Whereas, according to the concentration gradients, Mn(III)-L should be fluxing out of the sediments, the complex could not be detected in water immediately overlying the sediment-water interface. At Station 17, the flux of Mn(II) estimated from the concentration gradient between the top 0.5 cm of the sediments and the overlying water was 0.24 µmol cm^{-2} yr^{-1}, whereas the flux of Mn(II) estimated over the same vertical distance across the sediment-water interface at hypoxic Station 23 is 20 times greater (11 µmol cm^{-2} yr^{-1}), and 5-times greater than at SAG-30 (Table 2). This likely reflects the combined effect of low bottom-water dO_2 and high organic carbon accumulation rates at Station 23. The Mn(asc) accumulation rate (1.13 µmol cm^{-2} yr^{-1}) at Station 23 is only slightly different from previous measurements at this same site (1.51 µmol cm^{-2} yr^{-1}; Lefort, 2012, Belley et al., 2013) and burial rates are identical. At SAG-30, we also observe low Mn(asc) accumulation rates (0.36 µmol cm^{-2} yr^{-1}) and intermediate Mn(asc) burial rates (0.24 µmol cm^{-2} yr^{-1}) compared to Stations 23 (1.13 µmol cm^{-2} yr^{-1}) and 17 (0.23 µmol cm^{-2} yr^{-1}). This

may be due to the higher biological activity at this more terrestrially influenced site and/or to the differential organic carbon accumulation rate (oxidant demand) at each station. Despite the organic carbon being mostly terrigenous at SAG-30, its organic carbon accumulation rate is intermediate between station 23 and 17.

We also estimated the Fe(asc) accumulation and burial rates but cannot assess losses of dissolved Fe to overlying water as it was undetectable in overlying waters. Attempts to measure dissolved Fe fluxes in ex-situ whole core incubations have shown that they are below our detection limits (Lefort, 2012). Katsev et al. (2007) have suggested that dissolved Fe will not flux out of sediments if dO_2 exceeds 20 μM, due to its rapid oxidation and precipitation as authigenic oxides. At Station 17, we estimated the accumulation and burial rates of Fe(asc) at 1.04 and 0.84 μmol cm^{-2} yr^{-1} respectively, which reproduce values calculated in 2010 (0.85 and 0.92 μmol cm^{-2} yr^{-1} respectively). Our calculations yield identical accumulation and burial rates for Fe(asc) at Station 23 in 2010 and 2013 (19.8 and 21 (± 0.5) μmol cm^{-2} yr^{-1}, respectively). Likewise, we calculate similar accumulation and burial rates for Fe(asc) at SAG-30 (21.7 and 23.5 μmol cm^{-2} yr^{-1}, respectively).

3.5 Mn Total Methods Comparison

The dMn_T concentrations determined by the porphyrin method in all three sediment profiles reported in this study follow the distribution pattern of the dMn_T concentrations measured by flame AAS (Figure 2, B panels), but the former were 5 – 50 μM higher than the latter. Although these differences are not directly correlated to the [Mn(III)-L] in these samples, the discrepancy may be due to the precipitation of Mn(III)-L humic complexes that are insoluble at pH<2, as the flame AAS samples were acidified for sample preservation. Oldham et al. (2017a) found that up to 100 % of the Mn(III)-L complexes measured in the water column of the LSLE could be precipitated by acidification; thus, acidification likely removes some of the Mn(III)-L complexes present at this site. Many techniques for trace metal analyses employ acidification for sample preservation prior to storage, and we note that this may not be suitable for soluble Mn assays, particularly at sites where humic material is abundant.

4 Discussion

4.1 Stations 23 and 17

The soluble Mn speciation in the upper layer of the sediment at Station 23 (Figure 2, middle panel, B) reproduces some of the observations reported in Madison et al. (2013) from the same site. These observations include abundant Mn(III)-L complexes and the presence of high Mn(III)-L concentrations below the depth of the solid-phase Mn maximum. Although the Mn(III)-L conditional stability constants we measured ($\log K_{COND}$ = 11.17 – 11.47) fall within the range of those determined by Madison et al. (2013) ($\log K_{COND}$ = 11.10 – 11.60), the shape of our dissolved Mn speciation profile is dissimilar. We find a much shallower sub-surface dMn_T maximum (1 cm versus 12 cm in 2010, Madison et al., 2013), and we observe Mn(III)-L throughout the entire porewater profile, whereas previous work indicated a sharp Mn(III)-L peak at 2 cm depth which rapidly disappeared with depth. This discrepancy may be due to seasonal differences in sampling: previous sampling was conducted in July 2010, whereas this work was conducted in September 2014, or small-scale spatial heterogeneity of benthic colonization (Lefort, 2012; Belley et al., 2013). The higher soluble Mn maximum and greater Mn(III)-L concentrations in September may be consistent with the greater flux of Mn to the upper sediments from settling particles during the fall months, and/or perhaps the trends are triggered by the settling of autochthonous organic matter produced over the course of the ice-free season (Annane et al., 2015), resulting in greater oxidant demand and complexation of Mn(III).

In addition to seasonal changes, the effects of bioturbation may be important at this site, as well as at our two other sites, Stations 17 and SAG-30. At depth, the formation of Mn(III)-L complexes may be promoted by bioturbation as reduced Mn(II) can be oxidized by intrusions of O_2. The abiotic oxidation of Mn(II) by O_2 is slow but can be accelerated by adsorption onto mineral surfaces (Davies and Morgan, 1989), through bacterial mediation (Tebo et al., 1997; 2005), and/or via *in situ* ligand-promoted oxidation (Duckworth and Sposito, 2005; Parker et al., 2007). As light does not penetrate to the seafloor in our study areas, these observations could also be a manifestation of dark production of reactive oxygen species (ROS), such as O_2^-, and their reaction with Mn(II) (Hansard et al., 2001; Learman et al., 2011). Brendel and Luther (1995) observed the presence of H_2O_2 in salt marsh sediments, indicating that during the

reduction of O_2 to H_2O, ROS likely form. Thus, ROS are likely an important pathway in the formation of oxidized Mn species in our sediments. The potential effect of bioturbation on speciation profiles is supported by visible inspection of the cores through the clear core barrels of the multi-corer and the small scale (cm) spatial variability of the soluble Mn and Fe vertical profiles as well as dO_2 and Mn(II) fluxes (Lefort, 2012), particularly at Station 23.

Oldham et al. (2017a) observed that in most of the water column at Station 23 the dMn_T speciation was dominated by Mn(III)-L (52 – 86 % of dMn_T), except in surface (17.6 %) and bottom waters (2.0 %). dMn_T was highest in the overlying sediment-core water (2.93 μM, Oldham et al., 2017a) with dMn_T comprised entirely of Mn(II), indicating that dMn_T escaped from the sediment to the overlying waters as Mn(II). Oldham et al. (2017a) also reported the presence of a solid phase [MnO_x] (1070 nM) maximum 3 m above the sediment-water interface at this site. This implies that the Mn(II) escaping the sediment is rapidly oxidized. Mn(III)-L complexes are either decomposed/oxidized closer to the sediment-water interface or upon escaping the sediment, which may be why there is no observed Mn(III)-L immediately above the sediment-water interface (SWI). Webb et al (2005) observed that the oxidation of Mn(III)→Mn(IV) is more energetically favorable than Mn(II)→Mn(III), thus perhaps oxidizing bacteria are preferentially using Mn(III)-L as an electron donor. Our vertical sediment sampling resolution (0.5 cm) does not allow us to document these processes. As [Mn(asc)] in the 0 – 2 cm depth interval of the sediment is 5 – 10 times higher than in the deeper portions of the sediment column (Figure 2, middle panels; Table 1), oxidation of Mn(II,III) and the formation of MnO_x also occurs in the top layers of the sediment and is likely an important sink for dO_2 in these sediments. As MnO_x must be recycled rapidly across the oxic-suboxic interface in the sediment, it likely makes up a significant component of sediment diagenesis at this site. Although Station 23 is closer to terrestrial sources of Mn than Station 17, its organic carbon accumulation rate is four times larger and we observe a slightly shallower Mn(asc) maximum (0.5 – 1.0 cm versus 1.0 – 2.0) and a lower maximum [Mn(asc)] (37.7 μmol g^{-1} versus 62.6 μmol g^{-1}).

4.2 Saguenay Fjord

Unlike at Station 23, the water column in the Saguenay Fjord is well oxygenated (240 µM at the surface and 180 µM at the bottom). Oldham et al. (2017a) found that Mn(III)-L accounted for 9.5 – 70 % of dMn_T in the water column of SAG-30, and that Mn(II) accounted for 100 % of the dMn_T speciation in the overlying sediment-core water, in which, like at Station 23, the highest concentration (2.28 µM) was observed. The estimated dissolved Mn(II) flux at this station was 2.0 µmol cm^{-2} yr^{-1} (Table 2), ~ 5 times lower than at Station 23 but ~10 times higher than at Station 17. This flux likely reflects the combined effect of greater bottom-water dO_2 along with the higher percentage of organic carbon content (2.5 % compared to 1.5 % at Station 23, and 1.1 % at Station 17; Table 2) and oxidant demand of these sediments. The higher bottom-water oxygen concentration at this site compared to Station 23 likely promotes the oxidation of Mn(II) released from the sediments and its re-precipitation as MnO_x. The porewater dMn_T at SAG-30 (Figure 2, bottom panel, B; Table 1) is lower than at Station 23, but strong Mn(III) complexes (log K_{cond} >13.2) accounted for <2 to 16.4 % of dMn_T at this site. The presence of strong ligands may reflect the greater abundance of terrestrially-derived ligands in these sediments than at Stations 23 and 17, where strong porewater Mn(III)-L complexes were not detected. Likewise, the much lower MnO_x concentrations (5.9 – 21.6 nM) in the water column at SAG-30 than at Station 23 (Oldham et al, 2017a) may be due to the presence of more Mn(III)-L complexes at SAG-30, short-circuiting the complete oxidation of Mn(II) to MnO_x, or by higher amounts of organic ligands reductively dissolving MnO_x to produce Mn(III)-L complexes. It has already been shown that humic ligands can dominate Mn(III) complexation in oxic waters (Oldham et al., 2017b). Humic substances make up to 52 – 100 % of the sedimentary organic matter at SAG-30 (Tremblay and Gagné, 2007). Mn(III)-binding terrigenous ligands enter the Saguenay Fjord through surface runoff and nearby wetlands and ultimately accumulate in the sediments. This is supported by the observation of abundant strong Mn(III)-L complexes in the surface waters at site SAG-30 (Oldham et al., 2017a).

4.3 Mn and Fe cycling and interactions

The oxidation of dissolved Mn and Fe and subsequent particulate deposition is the primary source of Mn and Fe to the sediments, and this source decreases in magnitude away from terrestrial inputs (e.g. Boyle et al., 1977). The higher dMn_T compared to dFe_T at Stations 17 and

23 are consistent with the observation that dissolved Mn is more readily transported than Fe in the water column from the coast to the open ocean due to lower rates of abiotic oxidation on suspended solid phases (Boyle et al., 1977). Unlike the solid-phase Mn, whose concentration is lower in the sediment at Station 23 than at Station 17, the Fe(asc) concentration is higher at Station 23, and in fact, is higher at all depths than the solid-phase Mn concentrations. This is consistent with the closer proximity to terrestrial sources of Fe and the inability of Fe(II) to escape the sediment even under severe hypoxia in the overlying water column because Fe(II) is abiotically oxidized more readily than Mn(II). This is also reflected in the burial rates of Fe(asc), which are identical to the Fe(asc) accumulation rates and ~20 times higher at this site than for Mn(asc) (Table 2). Much of the dFe_T (and reactive Fe) at this site is being trapped as acid volatile sulfides (AVS) (Lefort et al., 2012) whereas dMn_T does not form sulfides and is therefore more readily released from the sediment (Mucci, 2004).

In contrast to Stations 23 and 17 where $dFe_T < dMn_T$ in all samples, at SAG-30, $dFe_T > dMn_T$ below 5 cm. In spite of this, Mn(III)-L complexes were stable, suggesting partial kinetic stabilization against reduction by Fe(II) (eq. 2).

$$\text{Mn(III)-L} + \text{Fe(II)} \rightarrow \text{Fe(III)-L} + \text{Mn(II)} \qquad (2)$$

The stability of strong Mn(III)-L complexes against reduction by Fe(II) has been demonstrated in surface waters of a wetland ecosystem (Oldham et al., 2017b) as well as against reduction by HS^- in the anoxic bottom waters of the Chesapeake Bay (Oldham et al., 2015; 2017c). In fact, % Mn(III) organic complexation in the porewaters at SAG-30 is higher than % Fe(III) complexation at all depths, indicating that the ligands in this system preferentially bind to Mn(III) than to Fe(III). This is consistent with results of the thermodynamic calculations of Luther et al. (2015) who found that the range of $\log K_{cond}$ for Mn(III)-L complexes is frequently greater than for Fe(III)-L complexes in the same samples and results of Parker et al. (2004) in the case of pyoverdine complexes. Despite the high concentration of dFe_T in these sediments, we note that rapid cycling is taking place, as we observe for example at Station 23, slightly higher Fe(asc) burial than accumulation rates. This likely reflects the formation and preservation of AVS, a significant component of Fe(asc), from the large reactive Fe pool and a fraction of the

more refractory solid Fe phases under anoxic conditions (Gagnon et al., 1995; Lefort et al., 2012) (Table 2). This indicates that the cycling of Fe in these sediments is rapid and a manifestation of bioturbation and high organic carbon turnover, which we would expect at a terrestrially influenced site. Consequently, we note that because of bioturbation these sediments are heterogeneous, and our flux estimates solely represent a one-dimensional snapshot of the elemental cycling and not a spatially-integrated value. Although we calculate trends, a more complete flux study would require multiple whole core incubations to fully capture the sedimentary redox cycling at these biologically heterogeneous sites.

Interestingly, at our most pelagic site, Station 17, Fe(III)-L complexes made up 96.5 – 100 % of the porewater dFe_T at all depths, suggesting that Fe(III)-L may not be used as much as Mn(III)-L as a potential electron acceptor in the degradation of organic material as the Mn(III)-L speciation is more variable with depth. Nevertheless, in the top 3 cm of sediment at this site, there is a loss of ~60 μmol g^{-1} Mn(asc) and ~60 μmol g^{-1} Fe(asc); below this depth, there is an increase in soluble Mn (0.1 to 48.0 μM), which exceeds the increase in soluble Fe (ND to 13.2 μM). Given that the concentrations of dissolved Mn and dissolved Fe are lower than the concentrations of their respective reactive solid phases, reductive dissolution of solid phases may not necessarily result in the buildup of soluble species in the porewater. For dFe_T, diffusion downwards occurs and results in the formation of AVS and pyrite, whereas dMn_T can either diffuse up and out of the sediment or downwards to ultimately co-precipitate with authigenic carbonates or adsorb onto AVS and sediment particles (Mucci, 2004). However, there is high % complexation of both porewater Mn and Fe at Station 17, suggesting that organic ligand concentrations are in excess of dissolved metal concentrations at this site, maintaining both species in the soluble phase. As Mn(III)-L complexes are being formed below the depth of Mn(asc) depletion, we suggest that more refractory solid phases of Mn below 3 cm depth are reductively dissolved by organic ligands, forming Mn(III)-L complexes, and that MnO_x is an important component of sediment organic matter decomposition at this site.

Hydrogen sulfide, a strong reducing agent for Mn oxides, was not detected in these sediment porewaters, which indicates that it is either titrated out by reaction with oxidized species of Mn and Fe, or that it is not formed in sufficient concentrations to significantly contribute to the

reduction of Mn. Gagnon et al (1995) proposed that the titration of hydrogen sulfide by dissolved Fe does not allow for its accumulation in sediment porewaters and consequently, there is no upward diffusion to the oxic layer. Additionally, since porewater Fe(II) (another reductant) concentrations were below our detection limit in the upper sediments (0 – 2.0 cm) at Stations 23 and 17, the reduction of MnO_x in these upper sediments is likely dominated by bacterially-mediated dissimilatory Mn oxide reduction. At SAG-30, we observed the Mn(asc) maximum at the shallowest, 0 – 0.5 cm, depth interval. The decrease in Mn(asc) coincided with the disappearance of dO_2. One possible explanation for this is the high accumulation rates of organic carbon in these sediments, coupled with the 2D heterogeneity of surface sediments at this site. Although MnO_x may be rapidly forming at the sediment surface, rapid reductive dissolution and complexation by terrestrial organic matter may subsequently dissolve these oxides, producing Mn(III)-L in surface sediments. Indeed, we see high concentrations of Mn(III)-L at shallower depths at this site than at Station 23 or 17, with > 90 μM Mn(III)-L in the 0.5 – 1.0 cm depth interval.

We did not observe detectable concentrations of Mn(III)-L complexes in the overlying water at any of our study sites, despite the presence of Mn(III)-L complexes in the upper sediment column and above the porewater Mn(II) maximum. This implies that Mn(III)-L complexes do not diffuse out of the sediment and may reflect the preferential use of Mn(III) by Mn-oxidizing bacteria given that Mn(III) is a more thermodynamically favorable electron donor than Mn(II) (Webb et al., 2005). We estimated an upward flux of soluble Mn(II) from the sediments to the water column at all three sites. This flux was highest at Station 23, consistent with previous findings, likely because of the lower bottom-water dO_2 concentrations at this station (Table 2). Consequently, dO_2 in the top 1.0 cm of this sediment is much lower than at our other two stations (ND in the 0 – 0.5 cm interval, Table 1). Lower dO_2 in the sediments and a thinner oxygen penetration depth results in greater loss of dissolved Mn to the overlying water column.

In Figure 3, the loss rates of Mn to the overlying water from this, and two other studies in the SLE are plotted against bottom-water dO_2. As anticipated, we see that higher fluxes of Mn(II) across the SWI correspond to lower overlying water dO_2. Thus, in areas of decreasing bottom-water dO_2 with sufficient sediment oxidant demand (or organic carbon accumulation rate),

greater mobility of dissolved Mn from the sediments to the water column is expected. In contrast, the residence time of Mn(II) above the sediment-water interface is likely a function of bottom-water dO_2. In the SLE, hypoxic bottom waters enriched in dissolved Mn and Mn-enriched fine-grained particles move landward (Sundby, 1977; Sundby et al., 1981). These waters are ultimately upwelled at the head of the Lower St. Lawrence Estuary (Gratton et al. 1988) and are ultimately transported seaward in surface waters, resulting in increased transport, beyond the river input of dMn_T from the coast to the open ocean (Sundby et al., 1981).

5 Conclusions

Our findings shed light on processes that couple the C, O, Mn, and Fe cycles during sediment diagenesis. We observe high concentrations of dissolved Mn(III)-L complexes throughout the sediment profiles of our three study sites. Based on our methodology, Mn(III)-L complexes do not appear to flux out of the sediments, implying that they are rapidly and preferentially consumed relative to Mn(II) during Mn oxidation. High porewater Mn(III)-L concentrations may also suggest that these potential electron acceptors play an important role in the degradation of organic matter upon the depletion of dO_2, particularly at sites with high organic matter content (as in Lin et al., 2012) and as electron donors in Mn oxidation to MnO_2 (Webb et al., 2005). We also find that Mn(III)-L and Fe(III)-L complexes coexist in the suboxic porewaters of the LSLE. Whereas sediment Fe(asc) concentrations exceed Mn(asc), peak dMn_T concentrations typically exceed peak dFe_T concentrations in the main estuary, suggesting that Mn-bearing solid phases are more readily dissolved to form soluble complexes. In the fjord, dFe_T exceeds dMn_T, and Fe(II) is a significant component of dissolved Fe speciation (up to 40 %). Nonetheless, we found up to 100 % Mn(III)-L complexation of porewater Mn at SAG-30, indicating that these Mn(III)-L complexes are kinetically stabilized to Fe(II) reduction (eq. 2), which may be similar to complexes in the anoxic bottom waters of the Chesapeake Bay that are kinetically stabilized against reduction by HS^- (Oldham et al., 2015). Two operationally-defined Mn(III)-ligand classes, weak and strong complexes, were detected and quantified in the sediment porewaters at the SAG-30 site, with the weaker complexes being likely more favorable electron acceptors in the microbially-mediated organic matter decomposition. The presence of these two classes of Mn(III)-L complexes in the Saguenay Fjord suggests that terrigenous ligands are more varied

and can bind Mn more strongly than ligands found in marine sediments further offshore. This is validated by the dissolved Mn speciation of sediment porewaters recovered in the LSLE and GSL, which only contained weak Mn(III)-L binding ligands ($\log K_{COND}$<13.2).

The Mn(III)-L complexes we measured at all three sites likely play a critical role in Mn cycling in these sediments, both as electron donors in the reoxidation of Mn(II) to MnO_2 in shallow sediments, and as electron acceptors in the microbially-mediated decomposition of organic matter. Porewater Mn fluxes out of the sediments solely as Mn(II) at all three study sites, but the flux is ~20 times larger at Station 23 in the LSLE than at Station 17 in the GSL, and ~5 times larger than at SAG-30. One possible interpretation is that Mn at Station 23 is more mobile because it is oxidized more slowly as it transits through the thinner and more oxygen-depleted upper portion of the sediments and the hypoxic overlying waters. The accumulation/delivery rates of Mn(asc) and Fe(asc) to the sediments decrease seaward, which is largely a function of the mass accumulation rate, whereas the loss of Mn to the overlying water should be related to the sediment oxygen penetration depth, itself a function of the overlying water dO_2 and the organic carbon accumulation rate. Because soluble Mn is transported further than Fe along estuarine gradients (Oldham et al., 2017b), soluble Mn, as Mn(III)-L complexes, likely plays an important role as a reactive intermediate in the breakdown of complex organic molecules (Lin et al., 2012), thereby presenting an unrecognized pathway as a regulator in global carbon cycling.

Acknowledgments

This work was funded by grants from the Chemical Oceanography program of the National Science Foundation (OCE-1558738 and OCE-1155385 to GWL; OCE-1558692 and OCE-1154307 to BMT) and the National Sciences and Engineering Research Council of Canada (NSERC) through Discovery and Ship-time grants to AM. Véronique Oldham thanks the University of Delaware for receipt of a Marian R. Okie Fellowship and a University of Delaware Graduate Fellowship. Thanks also to Gilles Desmeules as well as the captain and crew of the R/V *Coriolis II* who made sampling for this research possible.

References

Annane S, St-Amand L, Starr M, Pelletier E, Ferreyra GA (2015). Contribution of transparent exopolymeric particles (TEP) to estuarine particulate organic carbon pool. Mar. Ecol. Prog. Ser. 529: 17–34.

Anschutz P, Dedieu K, Desmazes F, Chaillou G. (2005). Speciation, oxidation state, and reactivity of particulate manganese in marine sediments. Chem. Geol. 218:265–279.

Barbeau C, Bougie R. Côté J-E (1981). Variations spatiales et temporelles du cesium-137 et du carbone dans les sédiments du fjord du Saguenay. Can. J. Earth Sci. 18: 1004–1011.

Beckler JS, Jones ME, Taillefert M (2015) The origin, composition, and reactivity of dissolved iron(III) complexes in coastal organic- and iron-rich sediments. Geochim. Cosmochim. Acta. 152: 72-88.

Bélanger C. (2003). Observation and Modelling of a Renewal Event in the Saguenay Fjord. Ph.D. thesis, Université du Québec à Rimouski, Rimouski, QC, 235 pp.

Belley R, Archambault P, Sundby B, Gilbert F, Gagnon J-M (2013). Effects of hypoxia on benthic macrofauna and bioturbation in the Estuary and Gulf of St. Lawrence, Canada. Continental Shelf Research 30:1302-1313

Benoit P, Gratton Y, Mucci A (2006) Modeling of dissolved oxygen levels in the bottom waters of the Lower St. Lawrence Estuary: coupling of benthic and pelagic processes. Mar. Chem. 102: 13-32.

Boyle EA, Edmond JM, Sholkovitz ER (1977). The mechanism of iron removal in estuaries. Geochim. Cosmochim. Acta, 41: 1313–1324.

Brendel PJ, Luther GW (1995) Development of a gold amalgam voltammetric microelectrode for the determination of dissolved Fe, Mn, O_2, and S(-II) in porewaters of marine and freshwater sediments. Environ. Sci. Technol. 29: 751–761.

Canfield DE, Jorgensen BB, Fossing H, Glud R, Gundersen J, Ramsing NB, Thamdrup B, Hansen JW, Nielsen LP, Hall POJ (1993). Pathways of organic carbon oxidation in three continental margin sediments. Mar. Geol. 11:27-40.

Chaillou G, Schafer J, Anschutz P, Lavaux G, Blanc G (2003). The behaviour of arsenic in muddy sediments of the bay of Biscay (France). Geochim. Cosmochim. Acta. 67:2993–3003.

Chen Q, Mucci A, Sundby B, Minarik W (2012) Early diagenesis of redox-sensitive elements in the Estuary and Gulf of St. Lawrence. Contributed poster presentation, 22st V.M. Goldschmidt Conference, June 24-29, Montréal, Canada. Mineralogical Mag. 76: 1568.

Chester R, Hughes MJ (1967). A chemical technique for the separation of ferro-manganese minerals, carbonate minerals and adsorbed trace elements from pelagic sediments. Chem. Geol. 2: 249–262.

Dellwig O, Schnetger B, Brumsack H, Grossart H, Umlauf L (2012). Dissolved reactive manganese at pelagic redoxclines (part II): Hydrodynamic conditions for accumulation. J. of Mar. Syst. 90: 31-41.

Dickie L, Trites RW (1983) The Gulf of St. Lawrence. In Estuaries and Semi-enclosed Seas, Edited by L. Dickie and R.W. Trites, Elsevier Scientific Publication, Amsterdam, pp. 403-425.

Duckworth OW, Sposito G (2005). Siderophore-manganese(III) interactions I. Manganite dissolution promoted by desferrioxamine-B. Environ. Sci. Technol. 39, 6045-6051

Edenborn HM, Mucci A, Belzile N, Lebel J, Silverberg N, Sundby B (1986) A glove box for the fine scale subsampling of sediment box cores. Sedimentology 33: 147-150.

El-Sahb MI, Silverberg N (1990) The St. Lawrence Estuary: introduction. In Oceanography of a Large-scale Estuarine System. Edited by M.I. El-Sabh and N. Silverberg, Springer-Verlag, New York, pp. 1-9.

Ferdelman G (1988). The distribution of sulfur, iron, manganese, copper, and uranium in a salt marsh sediment core as determined by a sequential extraction method. M.Sc thesis, University of Delaware.

Froelich PN, Klinkhammer GP, Bender ML, Luedtke NA, Heath GR, Cullen D, Dauphin P, Hammond D, Hartman B, Maynard V (1979). Early oxidation of organic matter in pelagic sediments of the eastern equatorial Atlantic, suboxic diagenesis. Geochim. Cosmochim. Acta. 43: 1075–1090.

Gagnon C, Mucci A, Pelletier E (1995) Anomalous accumulation of acid-volatile sulphides in a coastal marine sediment (Saguenay Fjord, Canada). Geochim. Cosmochim. Acta 59: 2663-2675.

Gaillard J-F, Pauwels H, Michard G (1989). Chemical Diagenesis in Coastal Marine Sediments. Oceanologia Acta. 12:175-187.

Gilbert D, Gobeil C, Sundby B, Mucci A, Tremblay GH (2005). A seventy-two year record of diminishing deep-water oxygen levels in the St. Lawrence estuary: The northwest Atlantic connection. Limnol. Oceanogr. 50: 1654-1666.

Genovesi L, de Vernal A, Thibodeau B, Hillaire-Marcel C, Mucci A, Gilbert D (2011). Recent changes in bottom water oxygenation and temperature in the Gulf of St. Lawrence: micropaleontological and geochemical evidence. Limnol. Oceanogr. 56: 1319-1329.

Gratton Y, Lefaivre D, Couture M (1994). Océanographie physique du fjord du Saguenay. Le fjord du Saguenay: Un Milieu Exceptionnel de Recherche, J.-M. Sévigny and C. M. Couillard, Eds., Ministère des Pêches et des Océans, Institut Maurice-Lamontagne, 8–16.

Gratton Y, Mertz G, Gagné, JA (1988) Satellite observations of tidal upwelling and mixing in the St. Lawrence Estuary. J. Geophys. Res. 93(C6): 6947-6954.

Hansard SP, Easter HD, Voelker BM (2011). Rapid reaction of nanomolar Mn(II) with superoxide radical in seawater and simulated freshwater. Environ. Sci. Technol. 45: 2811 – 2817.

Hedges JI, Keil, RG (1995) Sedimentary organic matter preservation: an assessment and speculative synthesis. Mar. Chem. 49: 81–115.

Hyacinthe C, Bonneville S, Van Cappellen P (2006). Reactive iron(III) in sediments: chemical versus microbial extractions. Geochim. Cosmochim. Acta 70: 4166–4180.

Katsev S, Chaillou G, Sundby B, Mucci A (2007). Effects of progressive oxygen depletion on sediment diagenesis and fluxes: a model for the lower St. Lawrence River Estuary. Limnol. Oceanogr. 52: 2555-2568.

Kostka J, Luther GW (1994). Partitioning and speciation of solid phase iron in salt-marsh sediments. Geochim. Cosmochim. Acta 58:1701–1710.

Lin H, Szeinbaum NH, DiChristina TJ, Taillefert M (2012). Microbial Mn(IV) reduction requires an initial one-electron reductive solubilization step. Geochim. Cosmochim. Acta. 99: 179-192.

Learman DR, Voelker BM, Vazquez-Rodrigues, Hansel CM (2011a). Formation of manganese oxides by bacterially generated superoxide. Nature: Geoscience. 4: 95 – 98.

Lefort S, Mucci A, Sundby B (2012). Sediment response to 25 years of persistent hypoxia. Aquat. Geochem. 18:461-474.

Lefort S (2012) Multidisciplinary study of hypoxia in the deep water of the Estuary and Gulf of St. Lawrence: Is this ecosystem on borrowed time? Ph.D. thesis, 149 pp., McGill University.

Leventhal J, Taylor C (1990). Comparison of methods to determine degree of pyritization. Geochim. Cosmochim. Acta 54: 2621–2625.

Locat J, Levesque C (2009). Le Fjord du Saguenay: Une physiographie et un registre exceptionnel. Revue des Sciences de l'Eau, 22: 135-157.

Luther GW, Kostka JE, Church TM, Sulzberger B, Stumm W (1992). Seasonal iron cycling in the salt-marsh sedimentary environment: The importance of ligand complexes with Fe(II) and Fe(III) in the dissolution of Fe(III) minerals and pyrite, respectively. Mar. Chem. 40: 81–103.

Luther GW, Sundby B, Lewis BL, Brendel PJ, Silverberg N (1997). Interactions of manganese with the nitrogen cycle: Alternative pathways to dinitrogen. Geochim. Cosmochim. Acta 61: 4043–4052.

Luther GW (2010) The role of one- and two- electron transfer reactions in forming thermodynamically unstable intermediates as barriers in multi- electron redox reactions, Aquat. Geochem. 16: 395–420.

Luther GW III, Madison AS, Mucci A, Sundby B, Oldham VE (2015). A kinetic approach to assess the strengths of ligands bound to soluble Mn(III). Mar. Chem. 173: 93-99.

Luther GW, Glazer BT, Ma S, Trouwborst RE, Moore TS, Metzger E, Kraiya C, Waite TJ, Druschel G, Sundby B, Taillefert ., Nuzzio DB, Shank TM, Lewis BL, Brendel PJ (2008) Use of voltammetric solid-state (micro)electrodes for studying biogeochemical processes: Laboratory measurements to real time measurements with an in situ electrochemical analyzer (ISEA). Mar. Chem. 108: 221-235.

Luther GW, Thibault de Chanvalon A, Oldham VE, Estes E, Tebo BM, Madison A (in press). Reduction of manganese oxides: thermodynamic, kinetic and mechanistic considerations for one- versus two-electron transfer steps. Aquat. Geochem. 54: 257-277.

Madison AS, Tebo BM, Luther GW (2011) Simultaneous determination of soluble manganese(III), manganese(II) and total manganese in natural (pore)waters. Talanta. 84: 374-381.

Madison AS, Tebo BM, Mucci A, Sundby B, and Luther III GW (2013). Abundant porewater Mn(III) is a major component of the sedimentary redox system. Science 341: 875-878.

Mucci A (2004) The behavior of mixed Ca-Mn carbonates in water and seawater: Controls of manganese concentrations in marine porewaters. Aquat. Geochem. 10:139-169.

Mucci A, Boudreau B, Guignard C (2003). Diagenetic mobility of trace elements in sediments covered by a flash flood deposit: Mn, Fe and As. Applied Geochem. 18: 1011-1026.

Mucci A, Richard L-F, Lucotte M, Guignard C (2000). The differential geochemical behavior of arsenic and phosphorus in the water column and sediments of the Saguenay Fjord Estuary, Canada. Aquat. Geochem. 6: 293-324.

Oldham VE, Owings SM, Jones M, Tebo BM, Luther GW (2015). Evidence for the presence of strong Mn(III)-binding ligands in the water column of the Chesapeake Bay. Mar. Chem. 171: 58-66.

Oldham VE, Mucci A, Tebo BM, Luther GW (2017a). Soluble Mn(III)-L complexes are abundant in oxygenated waters and stabilized by humic ligands. Geochim. Cosmochim. Acta. 199: 238-246.

Oldham VE. Miller MT, Jensen LT, Luther GW (2017b). Revisiting Mn and Fe removal in humic rich estuaries. Geochim. Cosmochim. Acta. 209: 267-283.

Oldham VE, Tebo BM, Jones MR, Luther GW (2017c). Oxidative and reductive processes contributing to manganese cycling at oxic-anoxic interfaces. Mar. Chem. 195: 122-128.

Parker D., Sposito G, Tebo BM (2004). Manganese(III) Binding to a Pyoverdine Siderophore Produced by a manganese(II)-Oxidizing Bacterium. Geochim. Cosmochim. Acta. 68: 4809–20.

Parker DL, Morita T, Mozafarzadeh ML, Verity R, McCarthy JK, Tebo BM (2007). Inter-relationships of MnO_2 precipitation, siderophore-Mn(III) complex formation, siderophore degradation, and iron limitation in Mn(II) oxidizing bacterial cultures. Geochim. Cosmochim. Acta 71: 5672-5683

Raiswell R, Canfield DE, Berner RA (1994). A comparison of iron extraction methods for the determination of degree of pyritisation and the recognition of iron-limited pyrite formation. Chem. Geol. 111: 101–110.

Reeburgh WS (1967). An improved interstitial water sampler. Limnol. Oceanogr. 12: 163–165.

Schafer CT, Smith JN, Côté R (1990). The Saguenay Fjord: A major tributary to the St. Lawrence Estuary. In: Oceanography of a Large-Scale Estuarine System: The St. Lawrence, M.I El-Sabh and N. Silverberg eds., vol. 39. New York, Springer-Verlag, 378-420.

Schulz HD (2000) "Quantification of early diagenesis: dissolved constituents in marine porewaters" in Marine Geochemistry, H.D. Shulz, M. Zabel, Eds., Springer.

Silverberg N, Bakker J, Edenborn HM, Sundby B (1987) Oxygen profiles and organic carbon fluxes in Laurentian Trough sediments. Netherlands Journal of Sea Research 21: 95-105.

Smith JN, Schafer CT (1999). Sedimentation, bioturbation, and Hg uptake in the sediments of the estuary and Gulf of St. Lawrence. Limnol. Oceanogr. 44: 207-219.

Smith JN, Walton A (1980). Sediment accumulation rates and geochronologies measured in the Saguenay Fjord using the Pb-210 dating method. Geochim. Cosmochim. Acta 46: 941–954.:

Stacey MW, Gratton Y (2001). The energetics and tidally induced reverse renewal in a two-silled fjord. J. Phys. Oceanogr. 31: 1599-1615.

Stookey LL (1970). Ferrozine. A new spectrophotometric reagent for iron. Anal. Chem. 42: 770-781.

Stone AT, Morgan JJ (1984). Reduction and dissolution of manganese(III) and manganese(IV) oxides by organics: 2. Survey of the reactivity of organics. Environ. Sci. Tech. 18: 617-624.

Sundby B (1977) Manganese-rich particulate matter in a coastal marine environment. Nature 270: 417-419.

Sundby B, Silverberg N, Chesselet R (1981) Pathways of manganese in an open estuarine system. Geochim. Cosmochim. Acta 45: 293-307.

Taillefert M, Bono AB, Luther GW (2000). Reactivity of freshly formed Fe(III) in synthetic solutions and (pore)waters: Voltammetric evidence of an aging process. Environ. Sci. Technol. 34: 2169–2177.

Taillefert M, Rozan TF, Glazer BT, Herszage J, Trouwborst RE, Luther GW (2002). Seasonal variations of soluble organic-Fe(III) in sediment porewaters as revealed by voltammetric microelectrodes, p. 247–264. In M. Taillefert and T. F. Rozan [eds.], Environmental Electrochemistry: Analyses of trace element biogeochemistry.

Tebo BM, Ghiorse WC, vanWaasbergen LG, Siering PI, Caspi R (1997). Review in Mineralogy. The Mineralogical Society of America. 35: 225 – 266.

Tebo BM, Johnson HA, McCarthy JK, Templeto, AS (2005). Geomicrobiology of manganese(II) oxidation. Trends in Microbiol. 13: 421 – 428.

Thibodeau B, de Vernal A, Mucci A (2006). Recent eutrophication and consequent hypoxia in the bottom waters of the Lower St. Lawrence Estuary: Micropaleontological and geochemical evidence. Mar. Geol. 231: 37-50.

Tremblay L, Gagné, J-P (2007) Distribution and biogeochemistry of sedimentary humic substances in the St. Lawrence Estuary and the Saguenay Fjord, Québec. Organic Geochemistry, 38: 682-699.

Trouwborst R.E, Clement B., Tebo BM, Glazer BT, Luther III GW (2006). Soluble Mn(III) in suboxic zones. Science 313: 1955-1957.

Van Cappellen P, Wang Y (1996) Cycling of iron and manganese in surface sediments: a general theory for the coupled transport and reaction of carbon, oxygen, nitrogen, sulfur, iron and manganese. Am. J. Sci. 296: 197–243.

van den Berg CMG (1995) Evidence for organic complexation of iron in seawater. Mar. Chem. 50: 139-157.

Webb SM, Dick GJ, Bargar JR, Tebo BM (2005) Evidence for the presence of Mn(III) inermediates in the bacterial oxidation of Mn(II). P. Natl. Acad. Sci. USA, 102: 5558-5563.

Yakushev EV, Pollehne F, Jost G, Kuznetsov I, Schneider B, Umlauf L (2007). Analysis of the water column oxic/anoxic interface in the Black and Baltic seas with a numerical model. Mar. Chem. 107: 388-410.

Yakushev E, Pakhomova S, Sørenson K, Skei J (2009). Importance of the different manganese species in the formation of water column redox zones: Observations and modeling. Mar. Chem. 117: 59-70.

Figures

Fig. 1 Map of the study sites in the St. Lawrence Estuary with an inset of the Saguenay Fjord site.

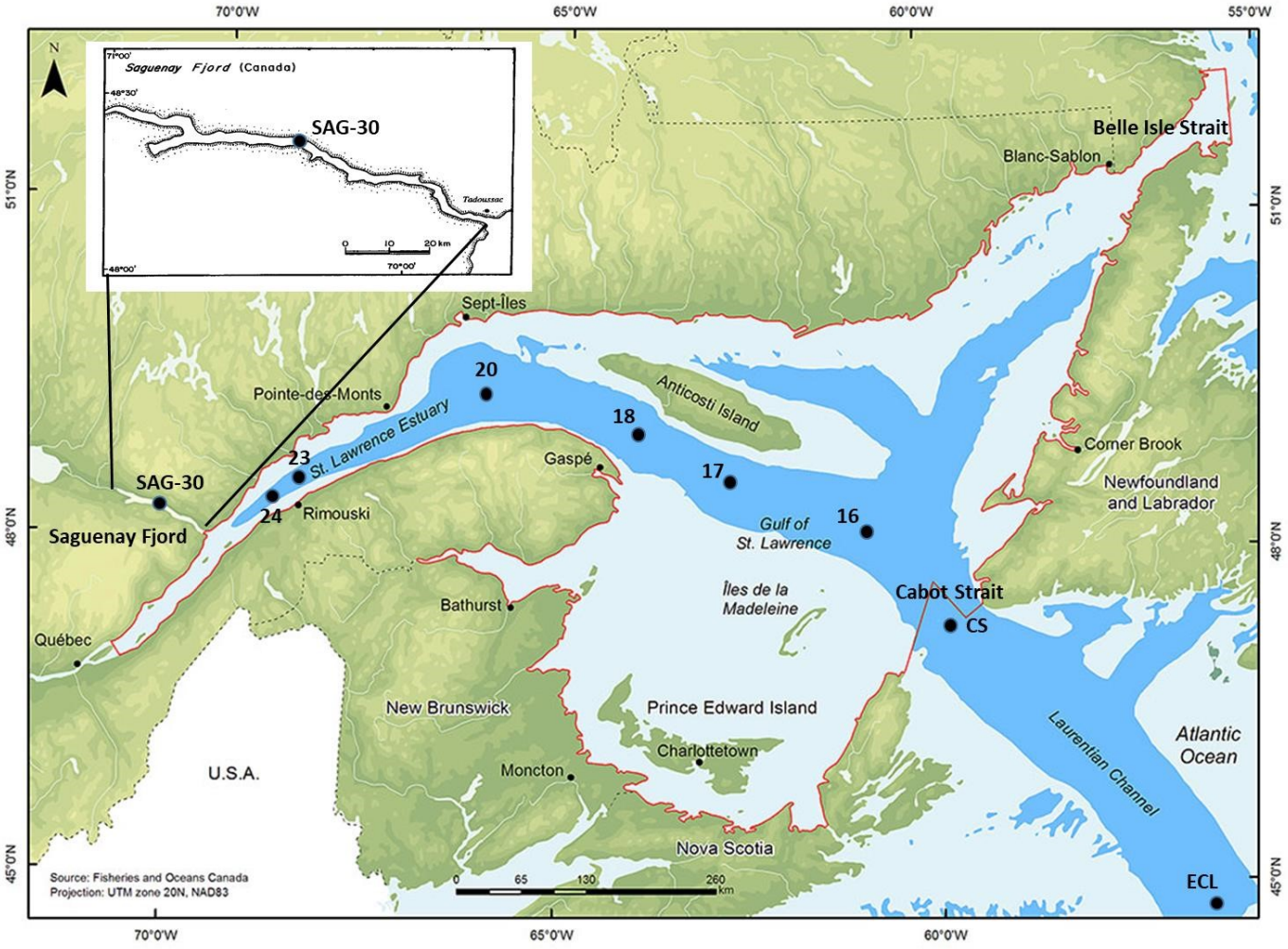

Fig. 2 Sediment porewater profiles for Station 17 (top), Station 23 (middle) and SAG-30 (bottom). Panels A (left) show dO_2 and solid MnO_x, Mn (asc) and Fe(asc). The "B" panels show dissolved Mn speciation by the porphyrin method and dMn_T by AAS. The "C" panels show dFe_T speciation by AAS (total) and ferrozine method (Fe(II)). Points above zero cm depth indicate data collected immediately above the sediment-water interface.

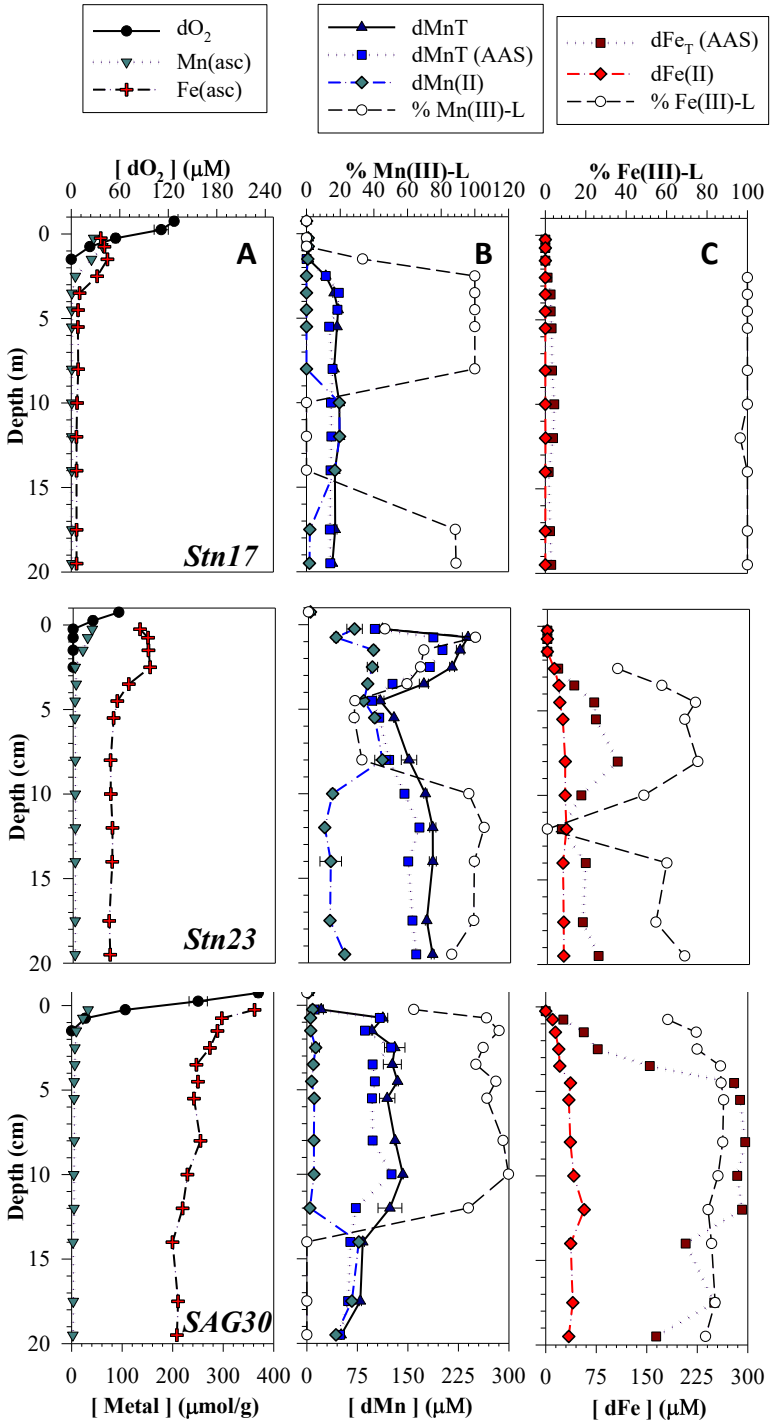

Figure 3 The loss of Mn from the sediments to the overlying water column from stations in the St. Lawrence Estuary with varying bottom-water oxygen concentrations. Data are from this study, Lefort et al (2012) and Silverberg et al (1985).

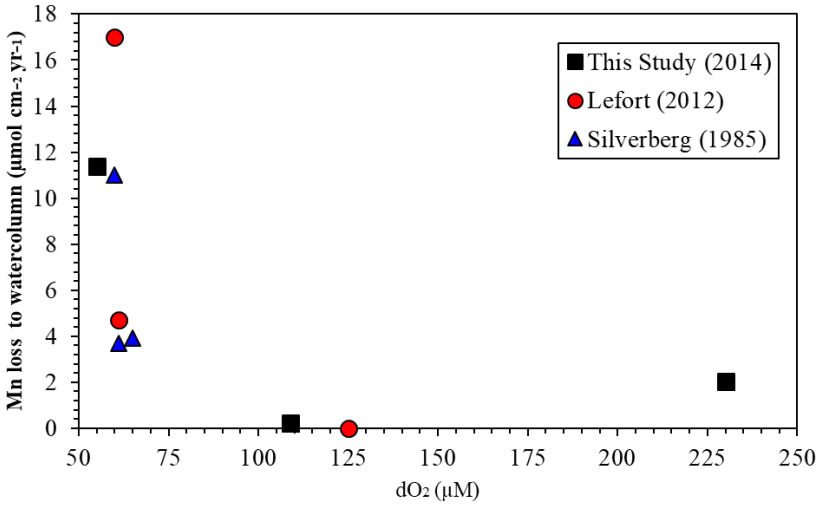

Table 1 Sediment porewater Mn speciation (in µM), conditional stability constants (log K_{cond}) for Mn(III)-L_{weak} complexes, dissolved Fe speciation (in µM; Fe(II) by Ferrozine assay and Fe(T) by flame AAS), and dO_2 (in µM) by high-resolution micro-electrode measurements. dMn_T represents the sum of Mn(II), Mn(III)-L_{weak} and Mn(III)-L_{strong}. Analyses for Mn(II) and Mn(III)-L_{weak} were performed without a reductant added, and their speciation was determined kinetically. Mn(III)-L_{strong} is calculated from the difference between the analyses of a sample prior to (Mn(II)+Mn(III)-L_{weak}) and after a reductant was added. Solid phases of Mn and Fe are given in µmol g^{-1}. Blank spaces designate samples where no analysis was made, and "ND" indicates samples where analyte concentration was below the detection limit. For each station, a dotted line designates the sediment-water interface (SWI), with data above the line representing solute concentration immediately (~0-10 cm) above the SWI.

Station	Depth (cm)	dO_2	dMn_T	dMn_T (AAS)	Mn(II)	Mn(III)-L_{weak}	$logK_{cond}$	% *Mn(III)-L_{weak}*	Mn(III)-L_{strong}	% *Mn(III)-L_{strong}*	Mn(asc)	Fe(II)	dFe_T (AAS)	Fe(asc)
17	(-1.0)-(-0.5)	127 ± 2	0.1 ± 0.0		0.1 ± 0.0	ND		*0.0*	ND	*0.0*				
	0.0	111 ± 9												
	0.0-0.5	55 ± 3	2.4 ± 1.4	0.1	2.4 ± 1.0	ND		*0.0*	ND	*0.0*	44.33	ND	ND	58
	0.5-1.0	23 ± 2	2.7 ± 1.0	0.1	2.7 ± 0.6	ND		*0.0*	ND	*0.0*	62.60	ND	ND	65
	1.0-2.0	ND	2.8 ± 0.3	0.1	1.9 ± 0.2	0.9 ± 0.2	11.70	*33.3*	ND	*0.0*	39.87	ND	ND	71
	2.0-3.0	ND	28.5 ± 1.3	28.5	ND	28.5 ± 0.9	11.44	*100.0*	ND	*0.0*	7.82	ND	3.3	51
	3.0-4.0	ND	40.8 ± 1.8	48.0	ND	40.8 ± 1.3	11.51	*100.0*	ND	*0.0*	1.13	ND	7.8	16
	4.0-5.0	ND	46.9 ± 2.0	45.9	ND	46.9 ± 1.4	11.51	*100.0*	ND	*0.0*	0.98	ND	8.0	13
	5.0-7.0	ND	45.2 ± 0.7	33.5	ND	45.2 ± 0.5	11.49	*100.0*	ND	*0.0*	0.95	ND	9.3	13
	7.0-9.0	ND	40.9 ± 1.6	38.7	ND	40.9 ± 1.1	11.46	*100.0*	ND	*0.0*	0.97	ND	9.9	14
	9.0-11.0	ND	48.6 ± 0.5	36.2	48.6 ± 0.2	ND		*0.0*	ND	*0.0*	0.92	ND	13.2	11
	11.0-13.0	ND	49.0 ± 0.1	36.9	49.0 ± 1.1	ND		*0.0*	ND	*0.0*	0.84	0.4 ± 0.4	11.4	10
	13.0-15.0	ND	42.0 ± 0.7	35.6	42.0 ± 1.3	ND		*0.0*	ND	*0.0*	0.99	ND	5.0	10
	15.0-18.0	ND	42.6 ± 2.6	34.6	4.9 ± 1.3	37.6 ± 2.1	11.23	*88.4*	ND	*0.0*	1.03	ND	7.0	10
	18.0-21.0	ND	38.3	35.2	4.3 ± 2.9	34.0 ± 2.0	11.17	*88.8*	ND	*0.0*	1.06	ND	8.8	10
23	(-1.0)-(-0.5)	57 ± 2	2.9 ± 0.0		2.9 ± 0.0	ND		*0*	ND	*0.0*				
	0.0	25 ± 3												
	0.0-0.5	ND	109.9 ± 4.4	98.5	68.4 ± 11.5	41.5 ± 8.6	11.45	*37.8*	ND	*0.0*	37.7	ND	ND	132
	0.5-1.0	ND	236.9 ± 8.4	185.5	41.1 ± 3.3	195.8 ± 22.1	11.43	*82.7*	ND	*0.0*	28.8	ND	ND	148
	1.0-2.0	ND	225.2 ± 5.5	199.0	96.5 ± 3.2	128.7 ± 1.1	11.39	*57.1*	ND	*0.0*	19.1	ND	ND	149
	2.0-3.0	ND	213.2 ± 3.6	180.2	94.9 ± 7.6	118.4 ± 3.0	11.32	*55.5*	ND	*0.0*	3.94	10.5 ± 0.5	16.1	152
	3.0-4.0	ND	171.4 ± 6.8	124.8	87.9 ± 0.6	83.5 ± 6.8	11.38	*48.7*	ND	*0.0*	5.93	17.3 ± 0.5	40.0	110
	4.0-5.0	ND	106.5 ± 5.5	94.1	82.0 ± 0.3	24.5 ± 4.3	11.43	*23.0*	ND	*0.0*	3.68	18.6 ± 0.2	69.5	87
	5.0-7.0	ND	126.8 ± 0.5	105.0	98.2 ± 3.0	28.7 ± 1.5	11.47	*22.6*	ND	*0.0*	3.42	23.1 ± 1.4	72.1	80
	7.0-9.0	ND	149.1 ± 11.4	119.6	109.8 ± 11.4	39.4 ± 1.0	11.23	*26.4*	ND	*0.0*	4.19	26.7 ± 0.8	104.5	74
	9.0-11.0	ND	173.7 ± 2.5	142.5	35.8 ± 3.5	137.9 ± 0.8	11.17	*79.4*	ND	*0.0*	4.17	26.4 ± 1.5	50.5	74
	11.0-13.0	ND	184.6 ± 4.6	164.7	24.1 ± 0.7	160.5 ± 6.5	11.20	*87.0*	ND	*0.0*	4.36	28.4 ± 1.5	21.6	78
	13.0-15.0	ND	184.7 ± 5.2	147.9	33.0 ± 16.0	151.6 ± 14.8	11.17	*82.1*	ND	*0.0*	4.02	23.3 ± 0.8	57.1	77
	15.0-18.0	ND	175.7 ± 2.2	154.3	31.9 ± 1.6	143.7 ± 1.2	11.23	*81.8*	ND	*0.0*	3.82	24.4 ± 0.1	52.7	71
	18.0-21.0	ND	184.5 ± 2.2	159.8	53.6 ± 3.1	130.8 ± 0.3	11.17	*70.9*	ND	*0.0*	3.76	24.4 ± 0.8	76.2	73
SAG30	(-1.0)-(-0.5)	231 ± 4	2.3 ± 0.0		2.3 ± 0.0	ND		*0.0*	ND	*0.0*				
	0.0	157 ± 11												
	0.0-0.5	66 ± 2	21.2 ± 3.3	10.9	8.5 ± 0.6	11.2 ± 0.5	11.40	*52.9*	1.5	*7.1*	32.6	ND	ND	362
	0.5-1.0	17 ± 3	112.8 ± 7.1	108.2	5.3 ± 0.4	100.3 ± 0.3	11.22	*88.9*	7.2	*6.4*	22.1	10.3 ± 0.4	26.1	297
	1.0-2.0	ND	96.5 ± 1.0	86.1	5.6 ± 1.1	90.9 ± 1.0	11.16	*95.2*	0.0	*0.0*	9.07	14.4 ± 0.7	56.7	288
	2.0-3.0	ND	130.4 ± 15.1	125.0	13.0 ± 5.7	113.8 ± 5.7	11.26	*87.3*	3.6	*2.7*	6.27	19.4 ± 1.5	77.3	273
	3.0-4.0	ND	126.9 ± 13.4	97.5	9.6 ± 1.5	106.1 ± 1.5	11.16	*83.7*	11.1	*8.8*	6.01	20.9 ± 0.8	154.6	247
	4.0-5.0	ND	134.6 ± 1.3	100.9	7.0 ± 0.7	125.9 ± 0.7	11.18	*93.6*	1.6	*1.2*	4.96	36.9 ± 0.1	279.6	250
	5.0-7.0	ND	119.2 ± 11.4	96.5	10.9 ± 0.9	106.2 ± 0.9	11.19	*89.1*	2.1	*1.7*	4.62	34.4 ± 0.5	288.5	242
	7.0-9.0	ND	130.9 ± 1.0	97.6	10.2 ± 1.1	120.6 ± 1.0	11.22	*97.1*	0.0	*0.0*	5.12	36.7 ± 0.7	296.1	255
	9.0-11.0	ND	142.4 ± 0.9	125.7	10.4 ± 0.9	131.9 ± 0.9	11.18	*99.8*	0.0	*0.0*	4.13	41.8 ± 1.6	284.4	229
	11.0-13.0	ND	123.2 ± 17.7	72.7	4.4 ± 0.6	98.5 ± 0.6	11.25	*80.0*	20.2	*16.4*	4.56	57.3 ± 2.3	291.5	220
	13.0-15.0	ND	82.8 ± 2.4	64.4	77.0 ± 0.0	ND		*0.0*	5.8	*7.0*	2.63	37.1 ± 3.2	207.8	200
	15.0-18.0	ND	79.3 ± 1.6	61.1	66.6 ± 0.1	ND		*0.0*	12.7	*16.0*	3.17	40.3 ± 1.0	250.2	210
	18.0-21.0	ND	50.7 ± 0.1	49.1	43.1 ± 0.1	ND		*0.0*	7.6	*15.1*	2.34	34.2 ± 2.3	164.0	208

Table 2 – Fluxes of Mn and Fe to and from the sediments at SAG-30, seaward of the Cabot Strait (CS) and ECL (Entrance of the Laurentian Channel). Calculations from this study were compared to data compiled from Mucci (2013, unpublished), Lefort (2012), Chen et al. (2012)

and Silverberg et al. (1987). In this table, SR = sedimentation rate, MAR = mass accumulation rate, OC = organic carbon, OC-AR = organic carbon accumulation rate. Values in bold are from this study.

	2010	2010	2010	2010	2010			Lefort (2012)	S&S (1985)	
Site	**SR**	**MAR**	**OC content**	**OC-AR**	**BW O_2**	**Mn(Asc) accumulation rate**	**Mn(Asc) burial**	**Mn loss to OLW**	**Mn loss to OLW**	**Fe(Asc) accumulati**
	cm/yr	**g/cm^2/yr**	**(wt%)**	**g-C/m^2/yr**	**(µM)**	**(µmol cm^{-2} yr^{-1})**	**(µmol cm^{-2} yr^{-1})**	**(µmol cm^{-2} yr^{-1})**	**(µmol cm^{-2} yr^{-1})**	**(mmol cm^{-2}**
						I-Mn(asc)/40 * SR				I-Fe(asc)/40 *
SAG-30	**0.23**	**0.12**	**2.5**	**30.5**	**230**	**0.36**	**0.24**			**21.7**
24	0.7	0.36	1.6	55.6	65	3.56	2.10		3.9	31.0
23	**0.5**	**0.29**	**1.5**	**43.6**	**55**	**1.13**	**1.10**			**19.8**
20	0.14	0.066	1.5	9.9	61	0.52	0.22	4.7	3.7	1.21
18	0.2	0.1	1.5	15.2	125	0.59	0.24			1.33
17	**0.15**	**0.088**	**1.14**	**10**	**139**	**0.227**	**0.104**			**1.04**
16	0.042	0.025	1.4	3.67	160	0.112	0.041	0		0.22
CS	0.011	0.0046	2.1	0.98	169	0.032	0.022	0		0.043
ECL	0.011	0.011	0.81	0.99	215	0.0058	0.0038	0		0.065